Prospects of Optimization of Energy Production by LIDAR Assisted Control of Wind Turbines

David Schlipf[1], Stefan Kapp[1] *, Jan Anger[1], Oliver Bischoff[1], Martin Hofsäß[1], Andreas Rettenmeier[1], and Martin Kühn[2]

[1] Endowed Chair of Wind Energy, Institute of Aircraft Design, Universität Stuttgart, Allmandring 5B, D-70569 Stuttgart, schlipf@ifb.uni-stuttgart.de

[2] AG Wind Energy Systems, Institute of Physics, Universität Oldenburg, Marie-Curie-Str. 1, D-26129 Oldenburg

Abstract

In the presented work two approaches to increase the energy production of wind turbines are studied assuming the usage of a wind speed measurement provided by a nacelle based LIDAR system: The first approach uses the knowledge of the incoming wind speed to assist variable speed control. The second approach uses the wind direction information measured by a LIDAR system for yaw control. From this first analysis only marginal benefit can be gained by the LIDAR assisted speed control, but an increase of energy production by a couple of percent can be expected by LIDAR assisted yaw control.

Keywords

wind turbine control, LIDAR assisted control, speed control, yaw control, energy optimization.

1 Introduction

In recent years LIDAR (Light detection and ranging) technology found its way into wind energy. The possibility to optimize the energy production by nacelle or spinner based LIDAR systems is an important issue. The presented work describes how wind characteristics, such as wind speed and direction, can be reconstructed from the limited provided information and how this information can be used in two applications:
Firstly, the theoretical potential to increase the energy production in the partial load region by tracking optimal inflow conditions is presented. Traditionally, the rotor speed is adjusted by changing the electrical torque depending on the rotor speed itself. Due to the inertia of the rotor, the speed adaptation to the changing inflow conditions is delayed. A predictive feed forward control strategy is proposed to exploit the benefit of the knowledge of the incoming wind. The strategy is tested using full turbulent wind fields and an aeroelastic simulation model of a $5\,\mathrm{MW}$ wind turbine. The wind information is obtained by simulating a LIDAR system with the LIDAR simulator presented in [1]. Former studies [2] presented benefits of up to 10%, using estimated wind speed from turbine signals, which motivated this work. Here the comparison to existing indirect speed control strategies only shows a marginal increase in energy output at the expense of significantly raised fluctuations of the generator torque.
Secondly, the benefit of LIDAR assisted yaw control is explored. Traditionally, the wind direction signal is measured at one single point by a nacelle mounted wind vane behind the blades. This signal is disturbed by interference effects of the rotor. A promising way to obtain a more accurate measurement of the incoming wind direction is to measure it over the full rotor plane ahead of the turbine by LIDAR. This work was motivated by [3], where a benefit of 10% has been achieved using estimated wind speed. To evaluate the benefit in energy output, measurements from a nacelle sonic anemometer are compared to a scanning LIDAR system installed on a $5\,\mathrm{MW}$ turbine [4]. The expected increase of the energy output is about one percent of the annual energy production of the wind turbine, when using the wind direction signal from the LIDAR system instead of the sonic anemometer.
Both analyses are based on the wind reconstruction method presented in the following section. Here LIDAR measurements and the wind field are modeled and then identified similar to the observer design method used in control theory.
This paper is organized as follows: Section 2 deals with the wind field reconstruction based on line-of-sight wind speeds. Section 3 describes how a LIDAR system can be used to assist the speed control. In Section 4 results for LIDAR assisted yaw are demonstrated and Section 5 concludes the paper.

*now with Robert Bosch GmbH

2 Wind Reconstruction

To be able to use LIDAR measurements in turbine control they first have to be analyzed. In this section a method is proposed to retrieve the necessary information for LIDAR assisted speed and yaw control from nacelle based LIDAR measurements.

2.1 The Cyclops Dilemma

LIDAR systems are able to measure the speed of aerosols by the Doppler shift in the frequency of backscattered light. The limitation to the line-of-sight direction causes a problem using a single nacelle or spinner based LIDAR system for wind turbine control. This is called the "Cyclops dilemma": As a Cyclops cannot see three-dimensionally with only one eye, it is not possible to measure a three-dimensional wind vector by only one LIDAR system. For reconstruction of the three dimensional wind vector, three LIDAR systems focusing on the same point with linearly independent laser beams are needed, as used in the Musketeer experiment [5]. Using one nacelle mounted LIDAR system, the two missing systems can be omitted by using either one of the following two assumptions:

1. no vertical and no horizontal wind component
2. no vertical component and homogeneous flow

In Figure 1 the effect of both assumptions is shown. In this case the 3D vectors in the location p_1 and p_2 (measured at the same height) should be reconstructed from the line-of-sight wind speeds $v_{los,1}$ and $v_{los,2}$. The first assumption yields a_{11} and a_{21} representing a horizontal shear. By the second assumption the resulting vectors a_{12} and a_{22} are equal representing a cross-flow, as homogeneous flow on each height was assumed.
The dilemma exists, as long as the LIDAR measurement is used for yaw and pitch control at the same time: If the first assumption is used to calculate the inhomogeneous inflow, perfect alignment is assumed. If the second assumption is used to obtain the misalignment, homogeneous flow is assumed.
Nevertheless, nacelle based LIDAR systems can provide a good estimate of wind characteristics such as wind speed, shear and wind direction, depending on the used assumptions. Those assumptions will be used to derive internal reduced wind and LIDAR models. These models can be used in an estimator and have to be designed depending on the application. The estimator will give a perfect estimation of the wind characteristics, if the simulation model coincide with the internal model. Depending on the robustness, the estimated values will differ from the real ones using real data or more complex simulations. This method will be explained in the remainder of this section.

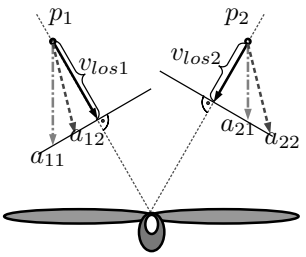

Figure 1: Ambiguity in wind reconstruction.

2.2 Models of the LIDAR Measurements

In a first step it is important to understand the problem introduced by the measurement technique. The LIDAR measurement of line-of-sight wind speed $v_{los,i}$ of each focus point $\begin{bmatrix} x_i & y_i & z_i \end{bmatrix}^T$ can be modeled by

$$v_{los,i} = l_{xi}u_i + l_{yi}v_i + l_{zi}w_i, \tag{1}$$

which is the projection of the wind vector $\begin{bmatrix} u_i & v_i & w_i \end{bmatrix}^T$ in the ith focus point on the normalized laser beam vector with focus length f_i:

$$\begin{bmatrix} l_{xi} \\ l_{yi} \\ l_{zi} \end{bmatrix} = \frac{1}{f_i} \begin{bmatrix} x_i \\ y_i \\ z_i \end{bmatrix}. \tag{2}$$

This equation shows how information is lost: For each measurement this model gives one equation with 3 unknowns (u_i, v_i, w_i) and therefore cannot be solved. By using three LIDAR systems focusing from linearly independent directions at the same focus point two equations can be added without new unknowns and the wind vector can be reconstructed with a unique solution.
It should be mentioned that (1) is very simplified due to the volume measurement of real LIDAR systems. The line-of-sight wind speed can be modeled more realistically by the following equation:

$$v_{los,i} = \int_{-\infty}^{\infty} (l_{xi}u(a) + l_{yi}v(a) + l_{zi}w(a)) f_L(a) da. \tag{3}$$

The weighting function $f_L(a)$ at the distance a to the focus point depends on the used LIDAR technology (pulsed or continuous wave). For the simulation in Section 3 and 4 a Gaussian shape weighting function with full width at half maximum (FWHM) of $W = 30\ \mathrm{m}$ is used, see Figure 2, following the considerations of [6] and [7]:

$$f_L(a) = \frac{e^{-4\ln 2(a/W)^2}}{\int_{-\infty}^{\infty} e^{-4\ln 2(a/W)^2} da} = \frac{2\ln 2 e^{-4\ln 2(a/W)^2}}{W\sqrt{\ln 2\pi}}. \tag{4}$$

LIDAR systems also provide further information such as turbulence broadening [8], which can be modeled and used to estimate the wind inflow. The method presented in this section is limited to the model (1).

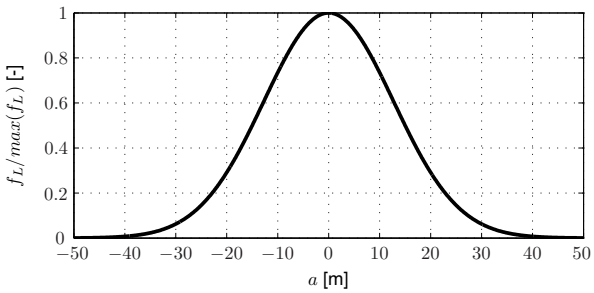

Figure 2: Normalized range weighing function $f_L(a)$ for the pulsed LIDAR system used in Section 3 and 4.

2.3 Wind Model v_0-δ_H-δ_V

In the first model, the wind direction is known and it is assumed that the wind is homogeneous in a vertical measurement plane in front of the turbine ($x_i = x \forall i$). For any known tilted inflow α_V or misalignment α_H the turbulent wind vector field is reduced to

$$\begin{bmatrix} u_i \\ v_i \\ w_i \end{bmatrix} = \begin{bmatrix} \cos\alpha_H \cos\alpha_V (v_0 + \delta_H y_i + \delta_V z_i) \\ \sin\alpha_H (v_0 + \delta_H y_i + \delta_V z_i) \\ -\sin\alpha_V (v_0 + \delta_H y_i + \delta_V z_i) \end{bmatrix}. \quad (5)$$

Following unknown wind characteristics are used: v_0 is the effective wind speed and δ_H and δ_V are the horizontal and vertical shear, respectively.
The advantage of this reduction is that various (n) measurements gathered simultaneously in the same measurement plane can be combined to get an estimation for the rotor effective wind characteristics. For non simultaneous measurements of scanning LIDAR systems, the last n focus points of a scan can be used. In both cases the focus points should be well distributed.
If, for example, it is assumed, that there is no tilted inflow and no misalignment ($\alpha_V = \alpha_H = 0$), following equations are obtained using (5), (1) and (2):

$$\underbrace{\begin{bmatrix} f_1 v_{los,1} \\ \vdots \\ f_n v_{los,n} \end{bmatrix}}_{m} = \underbrace{\begin{bmatrix} x & xy_1 & xz_1 \\ \vdots & \vdots & \vdots \\ x & xy_n & xz_n \end{bmatrix}}_{A} \underbrace{\begin{bmatrix} v_0 \\ \delta_H \\ \delta_V \end{bmatrix}}_{s}. \quad (6)$$

A solution for all three wind characteristics can only be found, if $rank(A) = 3$. If all measurements are obtained in one straight line, this condition is not fulfilled. For $n = 3$ there is one unique solution

$$s = A^{-1} m. \quad (7)$$

For $n > 3$ a solution can be selected by the method of least squares. If for example δ_H or δ_V is set to zero, because is assumed that there is no horizontal shear, there is no impact to the estimation of the other two unknowns. In a similar way a model v_0-α_H-α_V can be derived.

2.4 Wind Model v_0-α_H-δ_V

The second model also takes the unknown misalignment α_H of the turbine in consideration and assumes that there is no horizontal shear and no tilted inflow:

$$\begin{bmatrix} u_i \\ v_i \\ w_i \end{bmatrix} = \begin{bmatrix} \cos\alpha_H (v_0 + \delta_V z_i) \\ \sin\alpha_H (v_0 + \delta_V z_i) \\ 0 \end{bmatrix}. \quad (8)$$

Using (8), (1) and (2) a nonlinear equation system in v_0, α_H and δ_V is obtained, but similar to (6) a linear system in s can be formulated:

$$\underbrace{\begin{bmatrix} f_1 v_{los,1} \\ \vdots \\ f_n v_{los,n} \end{bmatrix}}_{m} = \underbrace{\begin{bmatrix} x & xz_1 & y_1 & y_1 z_1 \\ \vdots & \vdots & \vdots & \vdots \\ x & xz_n & y_n & y_n z_n \end{bmatrix}}_{A} \underbrace{\begin{bmatrix} v_0 \cos\alpha_H \\ \delta_V \cos\alpha_H \\ v_0 \sin\alpha_H \\ \delta_V \sin\alpha_H \end{bmatrix}}_{s}. \quad (9)$$

This system can be solved using the estimator (7), if $rank(A) = 4$. The wind characteristics can easily be calculated:

$$\begin{aligned} v_0 &= \sqrt{s_1^2 + s_3^2} \\ \alpha_H &= \arctan \frac{s_1}{s_3} \\ \delta_V &= \sqrt{s_2^2 + s_4^2}, \end{aligned} \quad (10)$$

with s_i the ith component of s. Again the solution for v_0 or α_H is not influenced, if δ_V is set to zero. In the same way a model v_0-α_V-δ_H can be defined.

2.5 Problems of Wind Model v_0-α_H-δ_H

Instead of, or in addition to δ_V, the horizontal shear can be included in the wind model (8):

$$\begin{bmatrix} u_i \\ v_i \\ w_i \end{bmatrix} = \begin{bmatrix} \cos\alpha_H (v_0 + \delta_H y_i) \\ \sin\alpha_H (v_0 + \delta_H y_i) \\ 0 \end{bmatrix}. \quad (11)$$

But when combining (11), (1) and (2) one obtains:

$$\underbrace{\begin{bmatrix} f_1 v_{los,1} \\ \vdots \\ f_n v_{los,n} \end{bmatrix}}_{m} = \underbrace{\begin{bmatrix} x & xy_1 & y_1 & y_1 y_1 \\ \vdots & \vdots & \vdots & \vdots \\ x & xy_n & y_n & y_n y_n \end{bmatrix}}_{A} \underbrace{\begin{bmatrix} v_0 \cos\alpha_H \\ \delta_V \cos\alpha_H \\ v_0 \sin\alpha_H \\ \delta_V \sin\alpha_H \end{bmatrix}}_{s}. \quad (12)$$

Due to the same x component, the second and third column are linear dependent ($rank(A) \leq 3$) and therefore α_H and δ_H cannot be estimated with the estimator (7). With a pulsed LIDAR system, it is possible to avoid this problem by measuring in different planes in front of the turbine and by combining those measurements, but this is beyond the scope of this work. The presented problem also holds for a model v_0-α_V-δ_V.

3 LIDAR Assisted Speed Control

The main goal of generator torque based speed control for variable speed wind turbines is to maximize the electrical power extraction below rated wind speed [9]. Therefore the turbine has to operate in the optimal aerodynamic range, hence at the optimal angle of attack at the rotor blades. This angle is represented by the ratio λ of the blade tip speed and the undisturbed rotor effective wind v_0:

$$\lambda = \frac{\Omega R}{v_0}, \tag{13}$$

where R is the rotor radius and Ω the rotor speed. The electrical power P_{el} below rated wind speed than can be modeled as

$$P_{el} = \underbrace{\frac{1}{2}\rho\pi R^2 v_0^3}_{P_0} c_P(\lambda)\eta, \tag{14}$$

where ρ is the air density, P_0 the power of the undisturbed wind, η the efficiency of the electromechanical energy conversion and $c_P(\lambda)$ the power coefficient, representing the aerodynamic-mechanical energy conversion depending below rated wind speed only on λ. The relation of the power coefficient and λ depends on the rotor design and is shown for the used $5\ \mathrm{MW}$ turbine model in Figure 3. The control goal to operate at the aerodynamic optimum can be refined to track the optimal tip speed λ_{opt} by adjusting the generator torque M_g. This section shows how tracking λ_{opt} can be improved by using the knowledge of the incoming wind and why, nonetheless, it cannot be recommended.

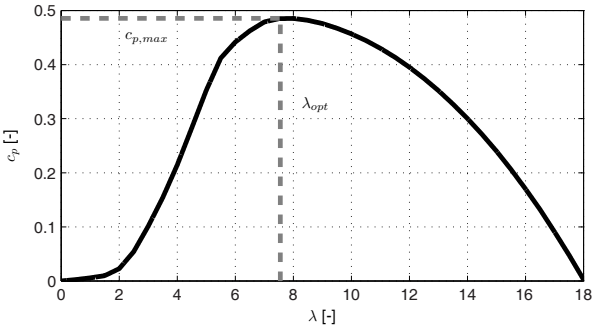

Figure 3: Power coefficient c_P over tip speed ratio λ of the used turbine.

3.1 Indirect Speed Control

The particularity of controlling λ is the high nonlinearity of the control task and that λ is not available under normal circumstances. Therefore a common output feedback controller such as PI-controller cannot be applied. Normally nonlinear state feedback controllers are used, measuring the generator or rotor speed.

For derivations of state feedback control laws, the following nonlinear reduced model of a turbine is chosen according to [10]:

$$J\dot{\Omega} = M_a(\Omega, v_0) - M_g/i$$
$$M_a(\Omega, v_0) = \frac{1}{2}\rho\pi R^3 \frac{c_P(\lambda)}{\lambda} v_0^2, \tag{15}$$

where M_a is the aerodynamic torque, i the gear box ratio and J is the sum of the moments of inertia about the rotation axis.

In steady state, the generator torque maintaining λ_{opt} can be determined by using (15) and (13):

$$M_{g,ISC}(\Omega) = \frac{1}{2}\rho\pi R^5 \frac{c_{p,max}}{\lambda_{opt}^3} i\Omega^2, \tag{16}$$

where all parameters are fixed, apart from the rotor speed. This equation is known as indirect speed control (ISC) and is normally applied for variable speed turbines.

Figure 4 shows the ISC [11], modified for transition from startup and to full load. The intersection of the state feedback law (solid) and the optimal, squared relation (dashed) is called "Region 2".

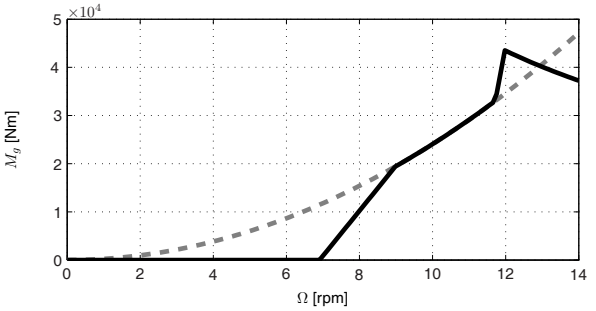

Figure 4: Optimal relation of rotor speed and generator torque (dashed), used state feedback (solid). Intersection: Region 2.

3.2 Direct Speed Control

By the LIDAR technology λ becomes measurable and therefore the proposed controller is considered as direct speed control (DSC).

A standard linear output feedback controller will not improve the performance due to the high nonlinearity. This becomes clearer, considering (15): The strategy,to reset λ as fast as possible after a positive wind step to its optimal value would be to lower M_g first to accelerate the rotor. If then λ_{opt} is reached, M_g has to be set to the value that stabilizes the optimal rotor speed and is above the value before the wind step. This behavior cannot be archived by a linear controller.

The basic idea of the proposed DSC is to keep the

ISC and to find a feed forward update to compensate changes in the wind speed similar to the one used for collective pitch control [12]. Therefore the error ε is introduced

$$\varepsilon = \Omega - \Omega_{opt}, \tag{17}$$

where the optimal rotor speed Ω_{opt} is defined as

$$\Omega_{opt} = \frac{\lambda_{opt} v_0}{R}. \tag{18}$$

Using (15) and (18), the dynamic of the error ε can be described by:

$$\dot{\varepsilon} = \dot{\Omega} - \dot{\Omega}_{opt} = \frac{1}{J}(M_a(\Omega, v_0) - M_g/i) - \frac{\lambda_{opt}}{R}\dot{v}_0. \tag{19}$$

With the proposed DSC

$$M_{g,DSC}(\Omega) = M_{g,ISC} - \underbrace{iJ\frac{\lambda_{opt}}{R}\dot{v}_0(\Omega)}_{M_{g,FF}} \tag{20}$$

the error dynamic is

$$\begin{aligned}\dot{\varepsilon}_{DSC} &= \frac{1}{J}(M_a(\Omega, v_0) - M_{g,ISC}/i) \\ &= \frac{1}{2}\rho\pi R^5\left(\frac{c_p(\lambda)}{\lambda^3} - \frac{c_{p,max}}{\lambda_{opt}^3}\right)\Omega^2.\end{aligned} \tag{21}$$

Similar to [13] it can be shown that $\dot{\varepsilon}_{DSC} < 0$ and $\varepsilon = 0$ as long as the tip speed ratio resides above a calculable lower limit. Therefore, in the nominal case, changes in the wind will be perfectly compensated by the feedforward part $M_{g,FF}$. For the non-nominal case, caused by inaccurate measurements or model uncertainties, the feedback part $M_{g,ISC}$ compensates deviations from optimal operation.

3.3 Simulation Results

To demonstrate the effect of wind gust tracking by the use of wind speed signals, a coherent gust (similar to [14], but with only $1\ \mathrm{m/s}$ amplitude) is applied to the reduced nonlinear system (15) of a $5\ \mathrm{MW}$ wind turbine and ISC and DSC are compared. As seen in Figure 5, ISC reacts to wind speed changes slowly as the rotor speed varies slowly. During the transition of the gust, the tip speed ratio departs from the optimum λ_{opt}, resulting in a suboptimal angle of attack at the rotor blades and thereby reducing power extraction from the wind. As opposed to this, feedforward based control, using a perfect wind speed signal, can indeed maintain the optimal operation of the turbine. However the generator torque M_g has to vary substantially to achieve the optimal lambda tracking and even is reaching negative values.

In a second step, a turbulent wind field with mean wind speed $\bar{u} = 9\ \mathrm{m/s}$ and a turbulence intensity of

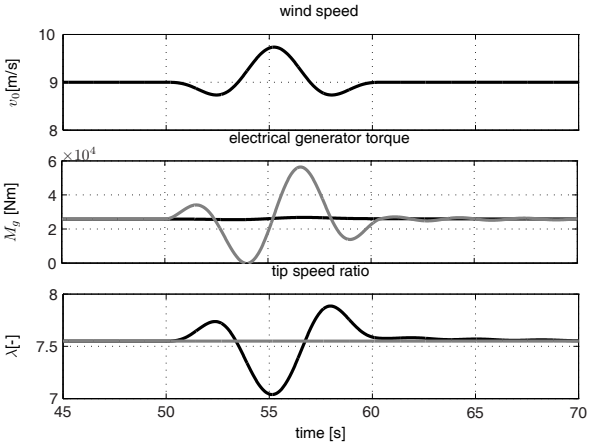

Figure 5: Reaction of the reduced model to a gust controlled by ISC (black) and DSC (gray).

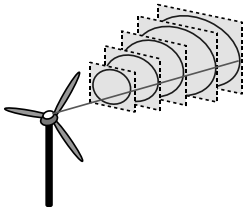

Figure 6: Circle trajectory used for speed control.

10% is created by TurbSim [15]. The low turbulence level is chosen to remain in Region 2 during the $10\ \mathrm{min}$ simulation. As simulation environment the FAST code [16] using a variable speed $5\ \mathrm{MW}$ wind turbine model [11] is coupled to the LIDAR simulator presented in [1], using a circle trajectory, see Figure 6. A rotor effective wind speed covering the rotor plane is calculated, using the model v_0-α-δ_V (5) and filtered (see Figure 7 top), applying a low-pass filter depending on the mean wind speed $\bar{u}$ of each wind field with cutoff frequency of

$$f_{\text{cutoff}} = \frac{\hat{k}\bar{u}}{2\pi}, \tag{22}$$

according to coherent turbulence structures up to $\hat{k} = 0.06\ \mathrm{rad/m}$ determined by a LIDAR mounted on a $5\ \mathrm{MW}$ wind turbine. In Figure 7 the improved tracking of λ_{opt} can be confirmed, as seen before in the gust simulation with the reduced turbine model. In Figure 8 the lower power spectral density (PSD) of the tip speed ratio applying direct speed control can be observed most notably for frequencies below f_{cutoff}. Therefore the standard deviation $\sigma(\lambda)$ is significantly reduced (see Table 1). However there is only a marginal increase in the energy production E_{el}. For this estimation the differences in rotational energy stored in the rotor are taken into account. Damage equivalent loads (DEL) for the low-speed shaft torque M_{LSS} are calculated based on a rainflow counting (Wöhler exponent of 4, lifetime 20 years, reference number of cycles $2 * 10^6$) and

show an increase of 34.7%.
In a third step, 33 simulations are performed by using turbulent wind fields (Weibull distribution with $C = 10\,\mathrm{m/s}$, $k = 2$ and wind turbulence class A according to [14]). Bins of $2\,\mathrm{m/s}$ from 4 to $24\,\mathrm{m/s}$ are chosen, each simulated with 3 different seeds. The feedforward control algorithm is only applied if a wind within Region 2 is detected by the simulated LIDAR. Also for this extended evaluation the lifetime weighted standard deviation for Region 2 $\sigma_{R2}(\lambda)$ can be reduced. But the marginal increase in energy extraction of 0.09% is bought dearly by increasing loads affecting the whole drive train including rotor shaft, gear box, generator and bearings, represented by the low-speed shaft torque M_{LSS}, where the DEL rise up to 8.9% (see Table 2).

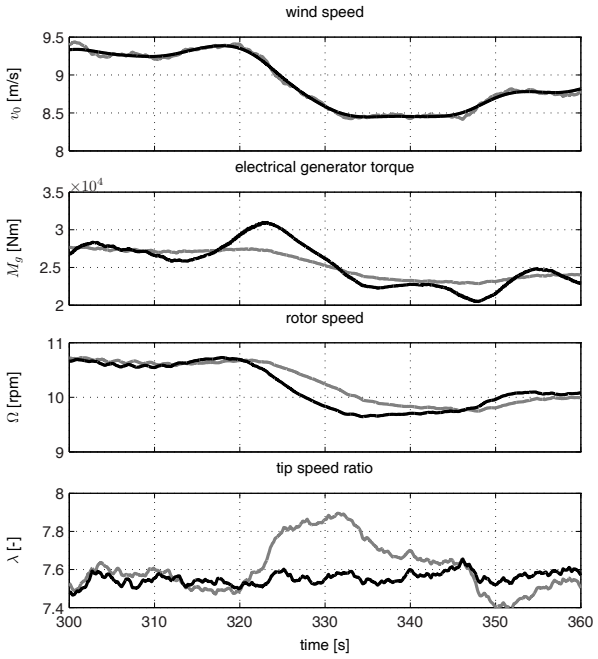

Figure 7: Top: Rotor effective wind speed (filtered: black). Rest: Reaction of the aeroelastic model: ISC (gray), DSC (black).

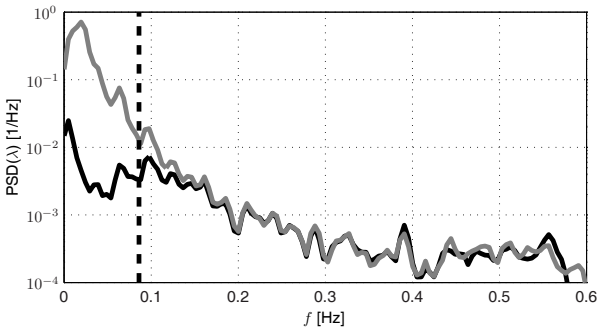

Figure 8: Power spectral density of the tip speed ratio: ISC (gray), DSC (black). Dashed: cut-off frequency of the wind speed filter.

	$\sigma(\lambda)$ [-]	E_{el} [kWh]	DEL(M_{LSS}) [MNm]
ISC	0.137	422.14	1.14
DSC	0.033	422.17	1.53
DSC/ISC [%]	24.1	100.01	134.7

Table 1: Comparison ISC and DSC for a $10\,\mathrm{min}$ simulation.

	$\sigma_{R2}(\lambda)$ [-]	E_{el} [GWh]	DEL(M_{LSS}) [MNm]
ISC	0.271	458.69	2.65
DSC	0.069	459.08	2.88
DSC/ISC [%]	25.6	100.09	108.9

Table 2: Life time comparison ISC and DSC.

3.4 Discussion

The fluctuation of the tip speed ratio can be used as a measure for the potential of energy optimization. Assuming the distribution of the tip speed ratio $\varphi_{\lambda_{opt};\sigma}$ to be Gaussian with mean λ_{opt} and a standard deviation $\sigma(\lambda)$, then the generated power can be estimated by

$$P_{el}(\sigma(\lambda)) = P_{el,max} \int_{-\infty}^{\infty} \varphi_{\lambda_{opt};\sigma(\lambda)} c_P(\lambda) d\lambda. \quad (23)$$

In Figure 9 this potential is quantified for the simulated wind turbine.

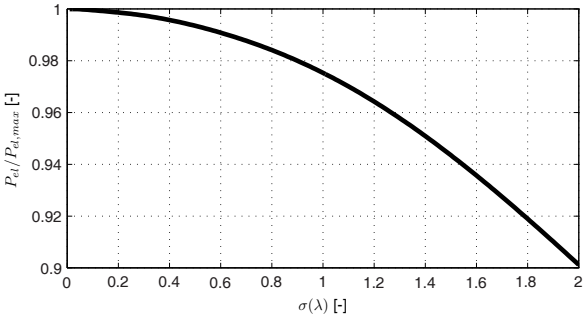

Figure 9: Relative power extraction by variation in tip speed ratio for the simulated turbine.

With (23) and the detected reduction of the tip speed ratio in Table 2 only an improvement in the energy production of 0.15% can be expected. Taking into account that by the given Weibull distribution, the turbine is only operating 19.0% of its lifetime in Region 2, this value is further reduced to 0.03%. The improvement of 0.09% in the energy production detected in the simulation is close to the expected value, considering the difficulty to detect such a small value.
Whereas the benefit of DSC should be irrelevant for all turbine sizes, the negative effect on loads should even increase for larger turbines due to the effect that the inertia J increases disproportionately.

4 LIDAR Assisted Yaw Control

Yaw control is usually done by active yaw control. Due to the large moment of inertia of the rotor about the yaw axis, the nacelle is aligned with the wind with slow rates and only, if the misalignment exceeds a certain value [17]. The demand signal is normally calculated from a nacelle mounted wind vane or sonic anemometer. There are mainly two disadvantages for these sensors: Firstly the signal is heavily disturbed for a operating turbine, e.g. by passing blades and therefore must be averaged over a certain time [9]. Secondly these sensors are measuring at one single point therefore are unable to detect changes over the rotor disc.
A nacelle mounted LIDAR system avoids these disadvantages, being able to measure the undisturbed inflow over the entire rotor area. Therefore using LIDAR technology has been proposed in literature for yaw control and the presented improvement in energy yield are promising and far exceed the estimated looses of 1 to 2% due to standard yaw control [17]. The first part of this section shows the capability and the problems of a simulated LIDAR system to capture the wind direction. In the second part data is analysed and finally in the third part the conditions for improvements in energy yield by LIDAR assisted yaw control are discussed theoretically.

4.1 Simulation Using Generic Wind

The scope of the presented simulation study is to test if the methods presented in Section 2 are robust and can be applied to turbulent wind fields. This is not obvious, because the simulation model of the wind (here IEC Kaimal [14]) and of the LIDAR ((3) and (4)) are more complex than the used design wind (8) and LIDAR model (1). Similar work has been presented [18], using an empiric reconstruction method and Mann turbulence.
The 33 Class A wind fields from section 3 are generated with a horizontal mean flow angle of $\alpha_H = 10\,\mathrm{deg}$. The $10\,\mathrm{min}$-wind fields are scanned again with the mentioned LIDAR simulator, imitating the SWE-LIDAR system [4] using a Lissajous-like trajectory, see Figure 10. Only the third measurement plane in $116\,\mathrm{m}$ is used, scanning a regular $87\,\mathrm{m}$ by $87\,\mathrm{m}$ grid with $n = 49$ focus points. The misalignment detected by the LIDAR $\hat{\alpha}_{HL}$ is estimated with the model (8) using those focus points from the last n points, where no impact with the turbine blades is simulated. Due to the positioning on top of the nacelle, similar to the one used in the experiment, this usually results in a loss of $\approx 30\%$.
The resulting $\hat{\alpha}_{HL}$ signal is very oscillating and for better illustration a $1\,\mathrm{min}$ running average is used in Figure 11. For comparison, the misalignment signal of a point measurement is plotted, which could be obtained from a sonic anemometer on hub height

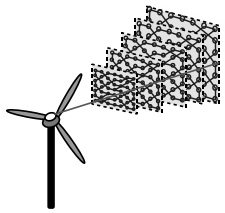

Figure 10: Optimized Lissajous-like trajectory used for yaw control.

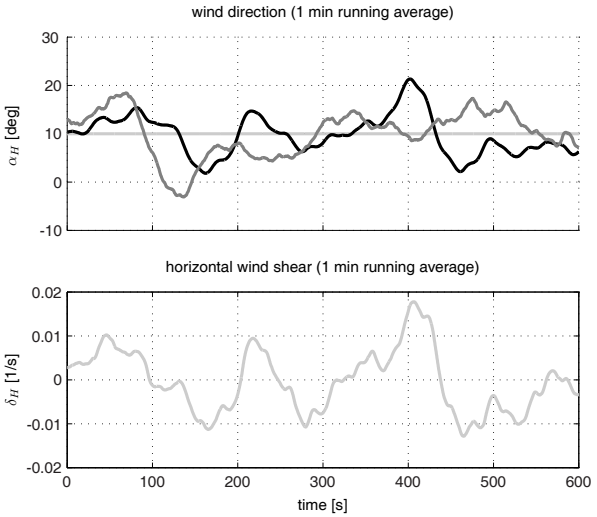

Figure 11: Misalignment and horizontal shear. From a wind field (light gray), LIDAR estimation (black) and sonic anemometer simulation (dark gray).

neglecting the disturbance of an operating turbine. Initially it seems that no advantage is gathered by the averaging over the rotor disc. But the reason for this effect can be observed in the running average of the effective horizontal shear from the wind field: The misalignment signal estimated with the LIDAR is disturbed by the horizontal shear, due to the effects described in Section 2.
However, Figure 12 shows that for all 33 simulations the error of the misalignment estimation in the $10\,\mathrm{min}$ mean is below $1\,\mathrm{deg}$ due to the fact that the mean of the effective horizontal shear for the wind field is close to zero. In the mean absolute error over the used 3 seeds a better estimation can be observed for higher wind speeds where the turbulence intensity of the wind fields is lower.
The results of this simulation study show that with the proposed method of wind reconstruction it is possible for a simulated LIDAR to estimate the misalignment of a turbine in the scale of $10\,\mathrm{min}$ similar to the simulated undisturbed sonic anemometer. An important requirement is that there is no constant horizontal shear, which is difficult to guarantee in complex terrain.

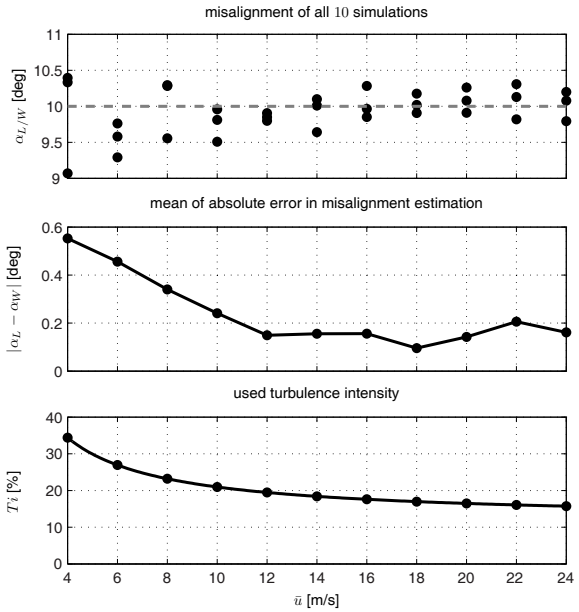

Figure 12: Evaluation of the simulation study for all 33 simulations.

Figure 13: SWE nacelle-based pulsed LIDAR system installed on a $5\ \mathrm{MW}$ turbine [4].

4.2 Simulation Using Real Data

From the simulation study above it is hard to estimate the improvement of LIDAR assisted yaw control compared to the standard yaw control: On one hand it is hard to model the disturbance which a nacelle mounted anemometer will experience in real conditions. On the other hand it is difficult to estimate the real wind direction in real experiments to evaluate the improvements.
Therefore, a simulation study is presented here using data from a real experiment: A scanning LIDAR system was developed and installed on a $5\ \mathrm{MW}$ wind turbine (see Figure 13) measuring the wind inflow. In the following investigation it is assumed that the LIDAR system is able to estimate the $10\ \mathrm{min}$ misalignment. This assumption is reasonable, considering the simulation study above and the location (flat terrain) where no constant horizontal shear is expected.
Data sets of at least $4\ \mathrm{h}$ are selected from almost 5 months of measurement using following criteria:

- Lissajous-like trajectory (see Figure 10)
- turbine in normal operation
- 50% of data availibility

By this procedure a total of $223\ \mathrm{h}$ is analyzed and the misalignment detected by the LIDAR $\hat{\alpha}_{HL}$ is again estimated using model (8).
In a first step the overall average is calculated: in the period of the $223\ \mathrm{h}$ an average misalignment of only $0.7\ \mathrm{deg}$ is detected. This shows, that no significant static misalignment can be detected. But this number is no indication, whether LIDAR assisted yaw control can reduce the fluctuation of the misalignment.
Therefore the basic idea of the second step is to analyze, how the wind direction tracking can be improved by the LIDAR compared to the sonic anemometer if the same yaw control strategy is applied, and if the LIDAR is able to perfectly estimate the misalignment. Therefore the absolute yaw direction signal γ_T is superposed with the relative, $10\ \mathrm{min}$ averaged misalignment signals from the nacelle mounted LIDAR and sonic anemometer to the absolute wind direction signals γ_L and γ_S from LIDAR and sonic anemometer, respectively. The assumed real wind direction γ is equal to γ_L, but $5\ \mathrm{min}$ shifted back in time, due to the assumption of the perfect LIDAR measurement and the delay of a $10\ \mathrm{min}$ average. Then following yaw control [17] is applied to γ_L and γ_S: The turbine yaws, if the absolute $10\ \mathrm{min}$ averaged misalignment is above $10\ \mathrm{deg}$. Starting for both instruments with no misalignment, the simulated turbine directions γ_{TL} and γ_{TS} are obtained. Figure 14 shows an extreme example of this method for better illustration.
With this method it can be simulated, how the turbine would have been yawed for both instruments. Finally, the resulting yaw misalignment for both instruments can be calculated by comparing the simulated turbine positions with the wind direction:

$$\begin{aligned} \alpha_{HL} &= \gamma - \gamma_{TL} \\ \alpha_{HS} &= \gamma - \gamma_{TS}. \end{aligned} \tag{24}$$

Due to the average time and the threshold in the control strategy, the difference in the fluctuation of both signals over the $223\ \mathrm{h}$ of data is relatively low: In this case the sonic anemometer assisted yaw control would have been achieved a standard deviation of $\sigma(\alpha_{HS}) = 6.4\ \mathrm{deg}$ and the LIDAR assisted yaw control despite of the perfect measurement a standard deviation of $\sigma(\alpha_{HS}) = 4.1\ \mathrm{deg}$.

4.3 Discussion

Both studies above show, the yaw misalignment can be divided in a static and a dynamic subproblem. In reality there will be a mixture of both, but this perception is helpful to rate the benefits which can be

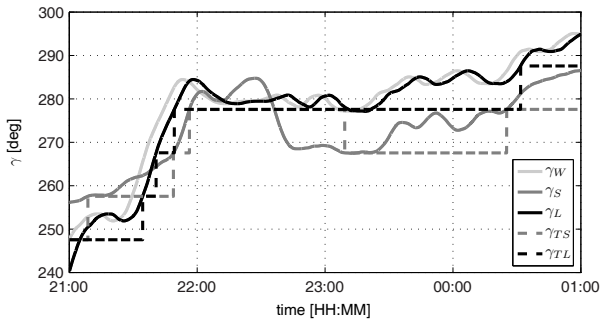

Figure 14: Measured wind directions and simulated yaw positions.

achieved by using a LIDAR system for yaw control. If there is a static misalignment $\bar{\alpha}_H$, the loss in power can be modeled as [9]:

$$P_{el}(\bar{\alpha}_H) = P_{el,max} \cos^3(\bar{\alpha}_H). \tag{25}$$

Figure 15, shows e.g. that $\approx 10\%$ of power is lost, if the turbine is misaligned by $\approx 15\,\mathrm{deg}$ to one side. This value can be considered as a lower bound, because a misalignment in full load operation will not have an effect on the power. Such a static misalignment could be caused by a miscalibrated anemometer or if the hub height wind direction has an offset compared to the rotor effective wind direction due to a very inhomogenious inflow e.g. in complex terrain. A static misalignment can be solved by better calibration of the standard nacelle anemometer and does not need a constant use of a LIDAR system. In the case of investigated data the detected static misalignment of $0.7\,\mathrm{deg}$ only would cause a power loss of 0.02%. This low value can be due to the fact that the considered turbine is a well calibrated prototype in flat terrain.
A constant use of a nacelle mounted LIDAR system is justified, if the fluctuation of yaw misalignment can be reduced. Similar to the discussion in Section 3.4 the misalignment can be assumed to be Gaussian distributed with zero mean and a standard deviation $\sigma(\alpha_H)$. Then the loss in power can be modeled by:

$$P_{el}(\sigma(\alpha_H)) = P_{el,max} \int_{-\infty}^{\infty} \varphi_{0;\sigma(\alpha_H)} \cos^3(\alpha_H) d\alpha_H. \tag{26}$$

The loss in power due to the dynamic misalignment is plotted in Figure 16 and again is only applicable to partial load operation. The reduction of $\sigma(\alpha_H)$ and therefore an improvement of the power output is limited to the control strategy: a reduction to $0\,\mathrm{deg}$ would require immediate yawing of the rotor which is neither feasible nor reasonable due to the induced loads. In the presented investigation a reduction from $6.4\,\mathrm{deg}$ to $4.1\,\mathrm{deg}$ yield to an improvement from $99.3\% - 98.2\% = 1.1\%$ using (26). This

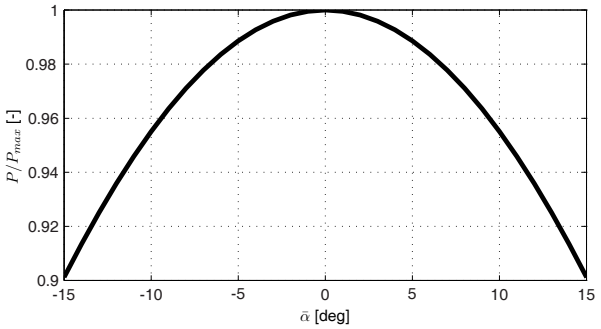

Figure 15: Power loss due to static misalignment.

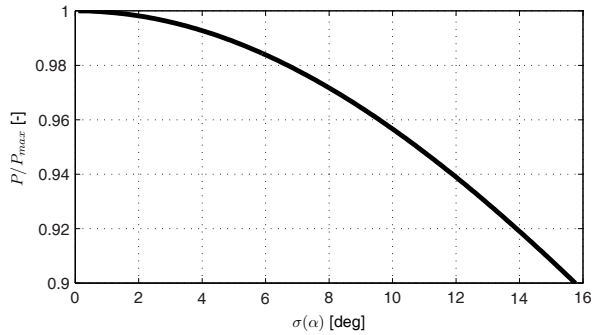

Figure 16: Power loss due to dynamic misalignment.

low value despite of assumed perfect reconstruction of the alignment by the LIDAR system can be due to the location but still gives an estimation of improvement which can be expected.
A validation of the LIDAR reconstructed rotor effective wind characteristics can be achieved by comparing to those estimated from turbine data. Figure 17 compares the shears obtained from model (5) with shears obtained by a zero-order estimation from blade root bending moment, showing as expected a better correlation for δ_V than for δ_H.

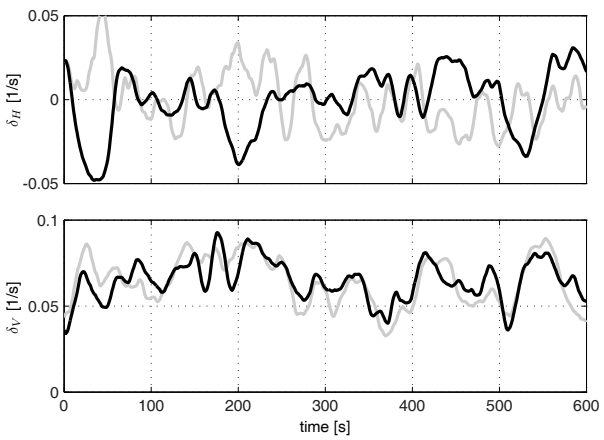

Figure 17: Estimated shears using LIDAR (black) and turbine data (gray).

5 Conclusion and Outlook

In this work a method is presented to reconstruct wind characteristics based on LIDAR measurements and shortcomings are shown. This method is used in two approaches to increase the energy production of wind turbines: The first approach uses the knowledge of the incoming wind speed to assisted variable speed control, but only marginal benefit can be gained. This is due to the fact that the standard variable speed control is already close to the aerodynamic optimum. The second approach uses the wind direction estimation by a LIDAR system for yaw control. Here an increase of energy production by a couple of percent can be expected, depending on the control strategy and the inhomogeneity of the wind.
To improve the wind reconstruction other spectral information of LIDAR measurements or a combination with blade root bending moment data should be considered and validated with turbine structural data.

Acknowledgment

This research is funded by the German Federal Ministry for the Environment, Nature Conservation and Nuclear Safety (BMU) in the framework of the German joint research project ”LIDAR II - Development of nacelle-based LIDAR technology for performance measurement and control of wind turbines” (FKZ 0325216B). Thanks to Björn Siegmeier from AREVA Wind GmbH for his help and the access to the turbine measurement data.

References

[1] Schlipf, D., Trujillo, J. J., Basterra, V., and Kühn, M., “Development of a Wind Turbine LIDAR Simulator,” *Proc. EWEC*, 2009.

[2] Boukhezzar, B. and Siguerdidjane, H., “Nonlinear Control of Variable Speed Wind Turbines without wind speed measurement,” *44th IEEE Conference on Decision and Control and European Control Conference*, 2005.

[3] Dakin, E., “Boosting Power Production, Project Report on Nebraska Public Power District, Vindicator LWS Field Trial,” *Catch the Wind, Inc.*, 2009.

[4] Rettenmeier, A., Bischoff, O., Hofsäß, M., Schlipf, D., Trujillo, J. J., and Kühn, M., “Wind field analyses using a nacelle-based LIDAR system,” *Presentation at EWEC*, 2010.

[5] Mikkelsen, T., Mann, J., Courtney, M., and Sjöholm, M., “Windscanner: 3-D wind and turbulence measurements from three steerable doppler lidars,” *IOP Conference Series: Earth and Environmental Science*, Vol. 1, No. 1, 2008, pp. 012018.

[6] Cariou, J. P., “Pulsed lidars,” *Remote Sensing for Wind Energy. Risøreport Risø-I-3184(EN)*, A. Peña and C. B. Hasager, June 2011, pp. 65–81, Risø-DTU.

[7] Lindelöw, P., *Fiber Based Coherent Lidars for Remote Wind Sensing*, Ph.D. thesis, Technical University of Denmark, 2008.

[8] Harris, M., “Introduction to continous-wave Doppler lidar,” *Remote Sensing for Wind Energy. Risøreport Risø-I-3184(EN)*, A. Peña and C. B. Hasager, 2011, pp. 41–64.

[9] Burton, T., Sharpe, D., Jenkins, N., and Bossanyi, E., *Wind Energy Handbook*, John Wiley & Sons, 2001.

[10] Bottasso, C. L., Croce, A., Savini, B., Sirchi, W., and Trainelli, L., “Aero-servo-elastic modelling and control of wind turbines using finite-element multibody procedures,” *Multibody Syst. Dyn.*, Vol. 16, 2006, pp. 291–308.

[11] Jonkman, J.; Butterfield, S.; Musial, W.; Scott, G., “Definition of a 5-MW Reference Wind Turbine for Offshore System Development,” *Technical Report NREL/TP-500-38060*, 2009.

[12] Schlipf, D., Fischer, T., Carcangiu, C. E., Rossetti, M., and Bossanyi, E., “Load analysis of look-ahead collective pitch control using LiDAR,” *Proc. DEWEK*, 2010.

[13] Johnson, K., Pao, L., Balas, M., and Fingersh, L., “Control of Variable-Speed Wind Turbines,” *IEEE Control Systems Magazine*, Vol. 06, 2006, pp. 70–81.

[14] “IEC 61400-1 third edition 2005-08 Wind turbines - Part 1: Design requirements,” 2005.

[15] Jonkman, J. and Buhl, M. L., “TurbSim User’s Guide,” Tech. Rep. NREL/TP-500-41136, NREL, April 2007.

[16] Jonkman, J. and Buhl, M. L., “FAST User’s Guide,” Tech. Rep. NREL/EL-500-38230, NREL, August 2005.

[17] Hau, E., *Windkraftanlagen*, Springer, 4th ed., 2008.

[18] Kragh, A., Hansen, M., and Mikkelsen, T., “Improving Yaw Alignment Using Spinner Based LIDAR,” *Proc. 49th AIAA Aerospace Sciences Meeting Including the New Horizons Forum and Aerospace Exposition*, 2011.